analytical chemistry

Article

Cite This: *Anal. Chem.* 2019, 91, 5621−5628

pubs.acs.org/ac

Acoustopipetting: Tunable Nanoliter Sample Dispensing Using Surface Acoustic Waves

Jasmine O. Castro,[†] Shwathy R. Ramesan,[†] Huy D. Dang,[‡] Amgad R. Rezk,[†] and Leslie Y. Yeo*[,†]

[†]School of Engineering, RMIT University, Melbourne, Victoria 3001, Australia

[‡]Invetech Pty. Ltd., Mount Waverley, Victoria 3149, Australia

ABSTRACT: We seek to demonstrate a robust, low-cost, and user-friendly acoustomicrofluidic platform that facilitates rapid, reproducible, and precise nanoliter sample dispensing. The solid-state chipscale platform exploits the unprecedented acceleration arising from high-frequency nanoelectromechanical vibrations, on the order of 10 million *g*, to jet the sample and hence generate a liquid bridge that spans across the substrate, on which the vibrations are generated and from which the sample originates, to a top target plate before rapidly pinching off to deposit the sample on the target with precise and reproducible volumes that can be tuned down to 0.22 μL with a standard error of 6.5% and coefficient of variation of 11.3%. The entire process occurs within approximately 10 ms. In addition to explicating the fundamental physical mechanism that underpins the technology, we demonstrate its use for serial dilution and concentration and, in particular, a cell-based drug toxicology assay. Moreover, we also show that multiple drop dispensing in an array, without requiring repositioning of the chip between dispensing steps, can be achieved through a simple but yet effective sequential directional jetting strategy, therefore allowing significant reduction in the total dispensing time in the case of massive-scale microarray operation. Given its low cost and compact size, the platform can easily be automated and parallelized, thus offering the prospect for introducing large-scale efficiencies in the laboratory workflow.

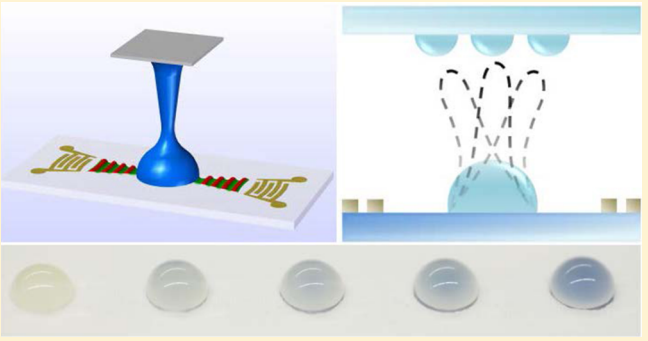

Miniaturization has increasingly been adopted across standard laboratory processes given the many advantages that working at smaller microscopic scales substantially offers. This includes reduced reagent consumption, increased sensitivity, and faster reaction times, among other benefits.[1−3] To this end, a number of microfluidic actuation schemes have been developed to facilitate fluid and particle handling at these scales.[2,4] Among these schemes, acoustics, in particular, surface acoustic waves (SAWs), which comprise nanometer scale electromechanical Rayleigh waves that propagate on the surface of a piezoelectric chip,[5] have been demonstrated as a powerful and versatile mechanism to drive a variety of microfluidic operations,[6−9] such as microchannel particle/cell trapping, sorting, and manipulation,[8,10−19] droplet transport,[20−25] microchannel/nanochannel actuation,[26−34] and microcentrifugation.[35−38] In addition, the unprecedented acceleration on the surface of the piezoelectric substrate as the SAW propagates across it, on the order of 10^8 m/s^2, has also proven to be extremely effective in ejecting liquid off its surface, whether through a jetting[39] or nebulization[40−44] process, therefore naturally lending themselves as platforms for improving sample dispensing precision and control at the nanoliter scale,[45] particularly for automated fluid transfer of small volumes onto or off chipscale devices or microarray plates.

SAW jetting, which can, among other ways,[46−48] be generated by applying an alternating electric field to opposing elliptical interdigitated transducer (IDT) electrodes to generate a focused pair of SAWs to a central point beneath a parent sessile liquid drop such that it gives rise to a converging flow within the drop with sufficient inertia to extend it upward as a filament, which, if unimpeded, proceeds to break up under capillary stresses to eject a single droplet or multiple droplets,[39] provides a convenient means for pipet- or nozzle-free liquid and cell printing applications.[49,50] If, on the other hand, a top plate is present at a small height above the SAW substrate such that the jet impinges onto it, a liquid bridge is generated, whose filament subsequently thins, necks, and pinches off under capillary action[51−53] to leave behind a small droplet on the plate (Figure 1a).

We shall show in this work that the volume of this spotted droplet can be flexibly tuned down to 0.22 μL such that the platform can be effectively exploited for efficient and precise pipet-free sample dispensing, for example, in plate-to-plate liquid transfer for serial dilution or concentration applications. Noting the extremely rapid (approximately 10 ms) time scale

Received: November 16, 2018
Accepted: March 27, 2019
Published: March 27, 2019

DOI: 10.1021/acs.analchem.8b05319
Anal. Chem. 2019, 91, 5621−5628

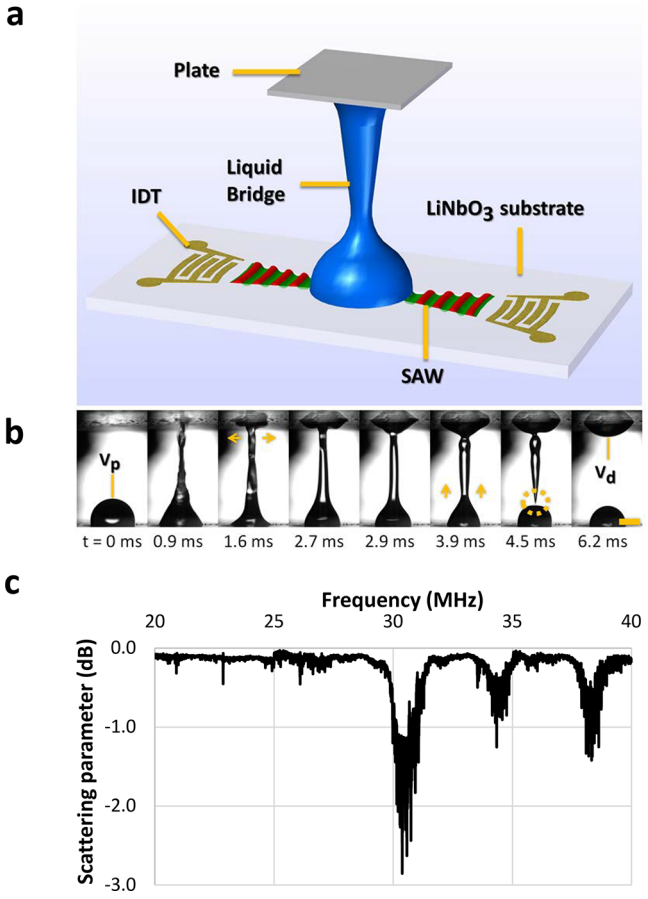

Figure 1. (a) Schematic illustration of the experimental setup (not to scale) showing two opposing SAWs, generated by applying an electrical signal to the focusing IDTs, that propagate along the surface, converging at the their focal point, above which a sessile parent droplet of volume V_p is placed. This gives rise to a jet, which impinges on the top plate to form a liquid bridge whose filament subsequently thins, necks, and eventually pinches off, leaving behind a dispensed residual droplet on the top plate with volume V_d, as captured by the time series of images obtained via high speed video in part b. In this case, a 50% DI water/glycerol solution was employed and the input power was approximately 6.0 W over a 1.25 ms pulse width; f_{SAW} = 30 MHz, V_p = 0.8 μL. The arrows illustrate the direction of the liquid flow and the scale bar denotes a length of approximately 1 mm. (c) Scattering parameter S_{11} as a function of the frequency, representative of the devices used in the study.

of the entire procedure, we importantly show that the liquid filament thinning, necking, and pinch-off dynamics is much faster than the droplet recoil speed such that there is negligible backflow of liquid from the target back to the source reservoir, therefore minimizing cross-contamination effects. Further, the process does not lead to denaturation of cells and large biological molecules.[49] Given its compact size and miniaturizability, the SAW chip can be mounted on a translation stage for automated control, in addition to its potential for being incorporated onto a dispensing array for massively parallel, individually addressable, sequential or simultaneous operation, on-demand.[54] Moreover, we shall also show the possibility of directional dispensing by tuning the jetting angle such that multiple droplets can be sequentially spotted in an array without requiring the SAW chip and hence the printhead to be moved, at least for the dispensing of a multiple set of droplets, thus facilitating quicker and more efficient printing when scaling out the dispensing process to accommodate large array handling.

METHODS

The focused SAWs are generated by applying a sinusoidal electrical pulse, produced through a signal generator (N9310A, Keysight Technologies Pty. Ltd., Mulgrave, VIC, Australia) and amplifier (ZHL-5W-1+, Mini-Circuits, Brooklyn, NY, USA), to the pair of elliptical IDTs (20 finger pairs with an eccentricity of 0.45 and a focal length of 2.5 mm; Figure 1), whose fabrication procedure onto the single-crystal 128° Y-X lithium niobate ($LiNbO_3$) chip of dimensions 23 mm × 10 mm × 0.5 mm has been documented elsewhere.[21,36,40] The gap between the finger electrode patterns of the IDTs specify a resonant SAW frequency $f_{SAW} \approx 30$ MHz, corresponding to a wavelength of $\lambda_{SAW} \approx 130$ μm, given the SAW velocity on the substrate of c_{SAW} = 3990 m/s; the reflection coefficient S_{11} for the devices used is shown in Figure 1c. The substrate surface is coated with a hydrophobic layer through vapor deposition of octadecyl(trichloro)silane[55] such that an aqueous sample of volume V_p between 0.5 and 1.0 μL placed on it results in a sessile parent drop, which when jetted upon excitation of the SAWs (a range of pulse widths and input powers between 0.35−1.25 ms and 2.3−38.6 W, respectively, were investigated) toward a parallel top plate comprising an uncoated microscope slide placed a small height above it (to avoid the formation of satellite droplets during the pinching of the jet, we limited the gap between the substrate and the top plate to a maximum of 4 mm), forms a transient liquid bridge, as depicted schematically in Figure 1a. To ensure reproducibility in the spreading of the liquid on the slide during the jetting process, the slide was carefully wiped clean prior to each run. The positioning of the parent drop on the substrate between the IDTs, to within ±1 mm of their geometrical focal point, can also be aided by confining them within bare (untreated) circular patches, achieved through masking (for example, covering it with a round piece of adhesive tape) during the silanization procedure.

The entire jetting process, and the subsequent thinning, necking, and pinching-off of the filament constituting the liquid bridge, can be seen in the series of images in Figure 1b, captured by a high speed video camera (SA5, Photron Ltd., Tokyo, Japan) at frame rates between 7 and 20 kfps, connected to a telescopic lens (K2 Objective CF-4, Edmund Optics Inc., Barrington, NJ). The image frames also reveal, at the top plate, the outward viscous spreading of a thin film due to the inertia of the jet as it impacts the plate at approximately t = 0.9 ms, which subsequently retracts slightly under capillarity as necking leading to pinching-off of the filament occurs at approximately t = 4.5 ms. Due to the pinch-off, the liquid on the top plate is isolated from the parent drop and forms an individual droplet constituting the deposited spot on the plate with a specific dispensed volume V_d, which we show below can effectively be tuned.

Liquids of different viscosities (0%, 33%, 50%, and 66% of deionized (DI) water/glycerol solutions, corresponding to viscosities of 1.005, 3.482, 8.365, and 26.613 cP at 20 °C, respectively)[56,57] were tested in order to demonstrate the reproducibility and precision across a range of liquids over which the sample can be reliably and accurately dispensed; for each of these samples, we did not observe any appreciable change in their initial contact angle of ≈90.9° ± 2.8° on the silanized substrate. Serial dilution was also conducted via

DOI: 10.1021/acs.analchem.8b05319
Anal. Chem. 2019, 91, 5621−5628

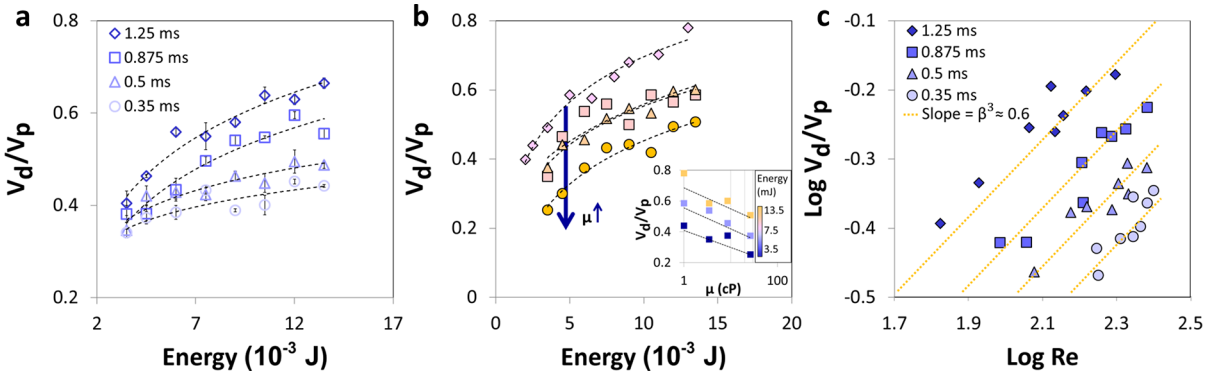

Figure 2. Dispensed droplet volume V_d, normalized against the initial parent drop volume V_p, as a function of the input energy, for (a) varying pulse widths for a 50% DI water/glycerol solution and (b) varying glycerol concentrations and hence viscosities μ (◇, 0% glycerol (1.005 cP); □, 33% glycerol (3.482 cP); △, 50% glycerol (8.365 cP); ○, 66% glycerol (26.613 cP)) for a fixed pulse width of 0.875 ms; the inset is a replot of the data with respect to the actual viscosity of the solutions. The error bars in part a show the standard error between measurements, which ranges from ±0.2% to ±6.5%, corresponding to coefficient of variation (CV) values of ±0.4% to ±11.3%, respectively. (c) Replot of the data in part a with respect to the Reynolds number Re showing the expected $Re^{3/5}$ behavior ($R^2 \approx 0.7-0.9$). The trendlines in parts a and b were added to guide visualization.

successive deposition of a DI water mixture with purple food dye using the technique; the concentration following each deposition step was subsequently evaluated in triplicates through a colorimetric intensity analysis using the software ImageJ (National Institutes of Health, Bethesda, MD). In this case, the top plate comprised a precoated Teflon glass microscope slide with bare 2 mm diameter circular patches (63434-02, Electron Microscopy Sciences, Hatfield, PA) onto which the droplets were dispensed.

The utility of the platform was further demonstrated for sample dispensing in a conceptual drug toxicity assay with human lung adenocarcinoma A549 cells tagged with green fluorescent protein (A549-GFP; Sigma-Aldrich Pty. Ltd., Castle Hill, NSW, Australia) and the chemotherapy drug paclitaxel (T7402; Sigma-Aldrich Pty. Ltd., Castle Hill, NSW, Australia). The cells were cultured in Roswell Park Memorial Institute Medium 1640 (RPM; Sigma-Aldrich Pty. Ltd., Castle Hill, NSW, Australia) and incubated at 37 °C, 5% CO_2. To conduct the assay, 5 mg/mL (5.8 mM) of paclitaxel was first diluted to a molarity of 5 nM. Subsequently, 4 separate droplets containing 4 μL of the cell solution at a concentration of 10^6 cells/mL were pipetted on the top plate, and different concentrations of paclitaxel were dispensed to each using the SAW with 1, 3, 5, and 7 repeats of the deposition events, each event dispensing approximately 0.5 μL of the drug solution. This results in a series of concentrations of paclitaxel within the cell solution that ranged from 0.6 to 2.33 nM, depending on the number of deposition events administered to each specific droplet containing the cell suspension. After exposure to the drug, triplicates of each concentration and the corresponding control solutions that were unexposed to the acoustic irradiation were transferred to a 96-well plate, where the culture media was reconstituted to 100 μL in each well. The cultures were then incubated for 48 h at 37 °C before the cells were assessed for viability using an MTT assay (3-(4,5-dimethylthiazolyl-2)-2,5-diphenyltetrazolium bromide; Sigma-Aldrich Pty. Ltd., Castle Hill, NSW, Australia).[58] The cytotoxicity level associated with each sample containing a different paclitaxel concentration was finally estimated through absorbance measurements of the solution at 570 nm (Spectramax Paradigm multimode plate reader, Molecular Devices LLC, Sunnyvale, CA), and the viability of the cells exposed to the drug was calculated as a percentage of that in the sham control in the absence of the drug. The entire procedure was also repeated for the case when the sample was dispensed via conventional manual pipetting for comparison (five individual samples for each concentration).

To measure the level of cross-contamination that may arise during dispensing, we jetted 2 μL of a 50% DI water/glycerol solution into 2 μL of fluorescein isothiocyanate (FITC, 4 mg/mL; Sigma-Aldrich Pty. Ltd., Castle Hill, NSW, Australia). A volume of 1 μL of the solution that remained in the parent drop was then transferred to a 96-well plate and diluted to 100 μL with DI water. Since the absorbance values obtained were close to that observed in the blank solutions, the samples were instead measured against a FITC detection curve to obtain the fluorescence detection limit at 490 and 530 nm, corresponding to the excitation and emission wavelengths of the FITC molecule, respectively. In addition, we also measured the typical level of contamination associated with the reuse of a pipet tip after a single contact dispensing event by repeating the aforementioned procedure using conventional manual pipetting.

Finally, to demonstrate multidirectional jetting and hence the ability to dispense several droplets in neighboring positions in the droplet array on the plate from a single position of the SAW chip, we tune the jetting angle with two variable attenuators (50R-193; JFW Industries Inc., Indianapolis, IN) connected by wires of identical length to each amplifier in order to modulate the power delivered to each IDT. Combinations of different powers were then applied to each opposing IDT by adjusting the attenuation to each from 0 to 10 dB, corresponding to a range between 100% and 10% of the original electrical signal, respectively. Besides measuring the resultant jet angle (triplicate measurements), we also acquired the surface displacement profile of the attenuated SAWs launched from each IDT using a laser Doppler vibrometer (UHF-120; Polytec Inc., Irvine, CA).

RESULTS AND DISCUSSION

Working Principle. Figure 2a shows that the volume of the dispensed droplet V_d is intricately tied to the volume of its parent source drop it originates from (V_p), the input energy to the SAW and hence the jet, which can be controlled through

DOI: 10.1021/acs.analchem.8b05319
Anal. Chem. 2019, 91, 5621−5628

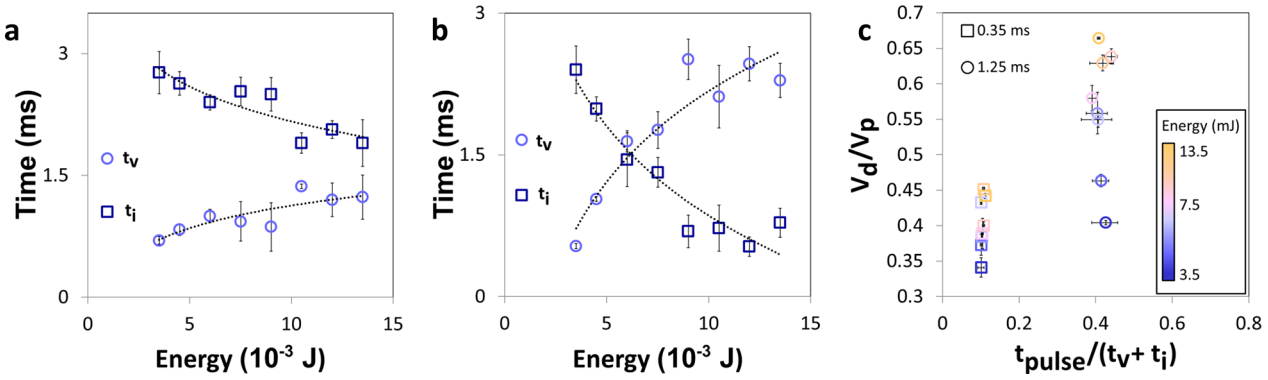

Figure 3. (a,b) Experimentally measured film viscous spreading time upon impact of the jet onto the target t_v and filament breakup time t_i as a function of the energy input into the system, which is calculated by multiplying the input power with the pulse width. The pulse width is 0.35 ms in part a and 1.25 ms in part b. (c) Normalized dispensed volume for the two values of the pulse width t_{pulse}, normalized against $t_v + t_i$ for different input energies. Error bars are based on the standard error, and the trendlines in parts a and b were added to guide visualization.

the input voltage applied to the IDTs, and the duration of the pulse over which this voltage is applied. For the liquid that was examined (50% DI water/glycerol), it was possible to tune the dispensing such that V_d varies from approximately 35% to 70% of V_p simply though these parameters. In the simplest sense, V_d is primarily controlled by the extent to which the liquid film that forms on the top plate (i.e., the target) spreads upon impact of the jet before the filament pinches off.

The dynamics that control this, however, are considerably more complex. Intensifying the SAW energy increases the inertial energy of the jet and hence its impact, leading to greater expansion of the thin film on the plate which, in turn, is modulated by viscous and capillary stresses that dissipate the inertial energy and retard the spreading of the film as well as its dewetting as it subsequently retracts under capillarity to form a pendant droplet.[59,60] Microscopically, the spreading and dewetting dynamics is also influenced by intermolecular forces, i.e., the disjoining pressure, at the advancing or receding film front, although for the partially wetting case of the plate surface, its weak logarithmic scaling suggests a negligible influence on the dynamic contact angle and the speed of the front compared to the viscous-capillary stress dominance;[61−63] we also note that the role of gravity is negligible given the small scales of the system (i.e., the Bond number $Bo \equiv \rho R_p^2 g/\gamma \ll 1$, wherein ρ is the liquid density, R_p the characteristic length scale of the parent drop, and g the gravitational acceleration).

Concurrently with the spreading and retraction of this impact film, the filament that makes up the liquid bridge also thins in parallel under capillary stresses, leading to its eventual breakup. The former, i.e., film spreading, is governed by a viscous−capillary time scale $T_v \sim \mu R_d/\gamma$ whereas the latter, i.e., the filament breakup, is governed by a capillary−inertia pinch-off time scale $T_i \sim (\rho R_d^3/\gamma)^{1/2}$; here, R_d denotes a characteristic droplet/film length scale, and μ and γ are the liquid viscosity and surface tension, respectively. For the system parameters we examine, $T_v \sim T_i \sim O(10^{-4} - 10^{-3}\ \mathrm{s})$. With increasing energy (input power multiplied by the pulse width) applied to the system, we expect the spreading time t_v to increase since the increase in the inertia of the jet and hence its impact force of the target leads to increased film spreading, whereas the filament lifetime t_i is expected to decrease due to faster pinch-off. This is, in fact, observed in Figure 3a,b, in which we also note that $t_v + t_i$ assumes a more or less constant value of approximately 3 ms, consistent with the viscous−capillary and capillary−inertia scaling above.

Given the comparable time scales, we note that the pulse width plays a critical role in the delicate balance between this capillary, viscous, and inertial stresses in the dynamic processes above by regulating the amount of inertial energy that is captured in the system. Should the pulse width be sufficiently short such that the jet loses its inertia while the impact film on the plate is still in its spreading phase, the droplet spreading is halted and hence less liquid is transferred from the parent drop through the liquid bridge to the spreading film on the target, leading to reduced droplet volumes V_d (Figure 3c). This dynamic can, in fact, be better characterized by a spreading parameter β which accounts for the maximum radius of spreading of the film R_{max}. For the viscous-dominated spreading in this work, a dominant force balance between the inertial, viscous, and capillary stresses leads to[59,64−66]

$$\beta \equiv \frac{R_{max}}{R_0} \sim Re^{1/5} \tag{1}$$

wherein R_0 is the initial radius of the droplet upon impact prior to its spreading and $Re \equiv \rho U R_0/\mu$ is the Reynolds number with U being the velocity of the jet. Given that it is not unreasonable to assume that R_0 is close to that of the initial filament that forms prior to its thinning and that this or the radius of the jet, which typically assumes a cylindrical shape,[39] is approximated by that of the parent drop on the substrate, it then follows that

$$\frac{V_d}{V_p} \sim Re^{3/5} \tag{2}$$

with which the data in Figure 2c is in decent agreement.

The effect of varying the liquid viscosity on the dispensing, on the other hand, can be seen more clearly in Figure 2b, although we note that the system behavior remains similar across the range of viscosities we investigated from 1.005 to 26.613 cP. Essentially, an increase in viscosity slows down the spreading and retraction of the impact film on the top plate, and its effects are typically akin to reducing the pulse width, thus further supporting the discussion above concerning the interrelationship between the pulse width and hence the inertia of the jet with the capillary−viscous spreading dynamics of the impact film on the filament breakup dynamics and thus the dispensed volume. In addition, we also note the reproducibility

DOI: 10.1021/acs.analchem.8b05319
Anal. Chem. 2019, 91, 5621−5628

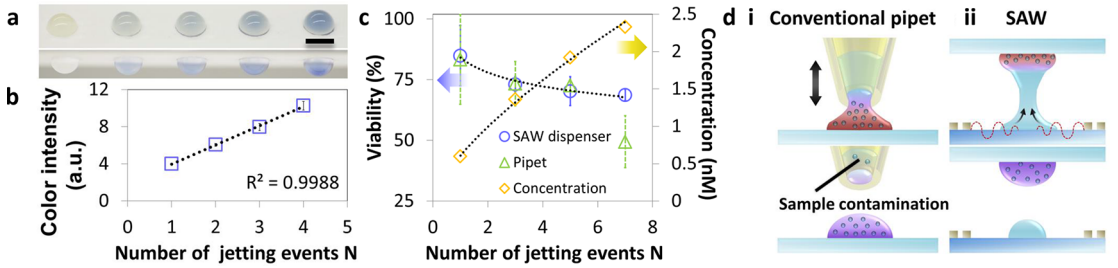

Figure 4. (a) Demonstration of serial dilution in target droplets on a top plate (top row, perspective view; bottom row, side view). Each droplet in the array has been dispensed with the same volume of purple dye from the source parent reservoir (whose volume V_p is held constant) repetitively over a number of times $N = n - 1$ associated with its position in the array n. For example, the third drop from the left ($n = 3$) was dispensed twice ($N = 2$) with a droplet of dye solution of the same volume V_d. The scale bar denotes a length of approximately 2 mm. (b) A corresponding colorimetric analysis of the droplets after the serial dilution process shows the dye concentration within them increasing linearly with a linear regression coefficient $R^2 = 0.9988$; the error bars represent the standard error in the experiment (±4.8%, corresponding to a CV of ±8.3%). (c) Results from a cell toxicity assay showing the decreasing viability of A549 cells in the target as the concentration of paclitaxel increases upon successive deposition of the drug with every dispensing event N compared to that achieved via manual pipetting; the trendlines were added to guide visualization. (d) Schematics illustrating (i) how sample cross-contamination arises in conventional pipets and (ii) why this is minimized with the SAW dispensing process.

and reliability of the present dispensing technique across a range of liquid viscosities (error and coefficient of variation (CV) below ±6.5% and ±11.3%, respectively), thus overcoming the limitation associated with mechanical dispensers where a combination of factors including capillary interactions between the sample and the walls of the pipet tip and electrical charging of these surfaces as well as that of the target substrate on which the sample is to be dispensed[67] can lead to staggering errors of up to 20%.[68]

Serial Dilution/Concentration and Sample Cross-Contamination. As an example of dispensing applications, we proceed to demonstrate the use of the platform for carrying out sample serial dilution and concentration, which are important and widely employed steps in the drug discovery workflow where testing of a drug response is carried out through an array of samples, each with varying concentration ratios.[69] To this end, successive jetting of a solution containing a purple food dye from a source with constant V_p onto a target droplet on the top plate can be seen to lead to its gradual dilution (Figure 4a), as verified by the linear increase in the color intensity of the droplet (Figure 4b); the R^2 value of 0.9988 obtained is comparable to that typically achieved with standard pipetting,[70] therefore attesting to the reproducibility of the platform to dispense the same volume repeatedly in order to obtain reliable and precise dilution profiles.

Given that the SAW itself does not lead to cell denaturation,[49,71] since the short milliseconds SAW pulses do not give rise to appreciable heating in the liquid, we also demonstrate the possible use of the platform for dispensing drugs with varying concentrations in a cell toxicity assay wherein a model chemotherapeutic agent was repeatedly dispensed to achieve varying concentrations in a droplet array containing A549 cells. Figure 4c shows the corresponding decreases in the cell viability with increasing drug concentration with a smaller standard error (±12.4%) compared to that obtained via conventional manual pipetting (±18.5%). Both methods can be seen to lead to similar values for the cell viabilities after each dilution step, although we observe manual pipetting to give a significantly lower value with a considerably larger error at the highest concentration. We also note the large error associated with the first dilution step for both techniques, which could have arisen due to poor mixing of the drug and the cell solution; with each subsequent dispensing event, however, the mixing that arises due to the fluid motion generated by the dispensing action can be observed to progressively reduce the error.

Sample cross-contamination, also known as sample carryover, is a cause of considerable concern, particularly in biological assays. In conventional (e.g., air- or positive-displacement) pipets, this commonly arises as a consequence of the repetitive aspiration and blow-out sequences recommended in standard pipetting techniques (Figure 4d). In order to quantify the extent of cross-contamination between the source on the SAW substrate and the target droplet on the plate, we examined the fluorescence intensity in a source parent drop containing a glycerol/water solution after it was dispensed into a target of FITC solution and found this to be negligible (<0.3%), as with other noncontact-free dispensing techniques, in comparison to that obtained via conventional manual pipetting (±1.0%), although we note the latter to be critically dependent on the operator. Despite the formation of a liquid bridge, the present technique is therefore comparable to other contact-free dispensing technologies. This is because the inertial time scale at which the jetting occurs, from which the liquid bridge is formed as well as the time scales over which the filament thins, necks, and pinches off, i.e., $T_i \sim O(10^{-4} - 10^{-3}\ \mathrm{s})$, are significantly shorter than either the viscous time scale associated with the retraction of the impact film along the surface target plate $T_r \sim \mu R_d^2/H_d\gamma \sim O(10^{-2}\ \mathrm{s})$, or the diffusional time scale over which molecular mixing across the filament occurs $T_d \sim L^2/\mathcal{D} \sim O(10^3\ \mathrm{s})$; here, H_d is the characteristic thickness of the film on the target, L the characteristic filament length, and $\mathcal{D}$ the diffusion coefficient. As such, there is insufficient time for backflow of liquid from the deposited droplet back to the source parent drop before the liquid bridge collapses on the pinch-off of the filament, therefore isolating both the source and target completely (Figure 4a). This is, in fact, evident from the images of the dispensing process in Figure 1b, as seen from the converging tail of what constitutes the remnant of the liquid filament at the onset of pinch-off at t = 4.5 ms (circled region) when the bridge detaches from the parent drop (were backflow to be present, a protrusion would instead be evident at the tail).

DOI: 10.1021/acs.analchem.8b05319
Anal. Chem. 2019, 91, 5621−5628

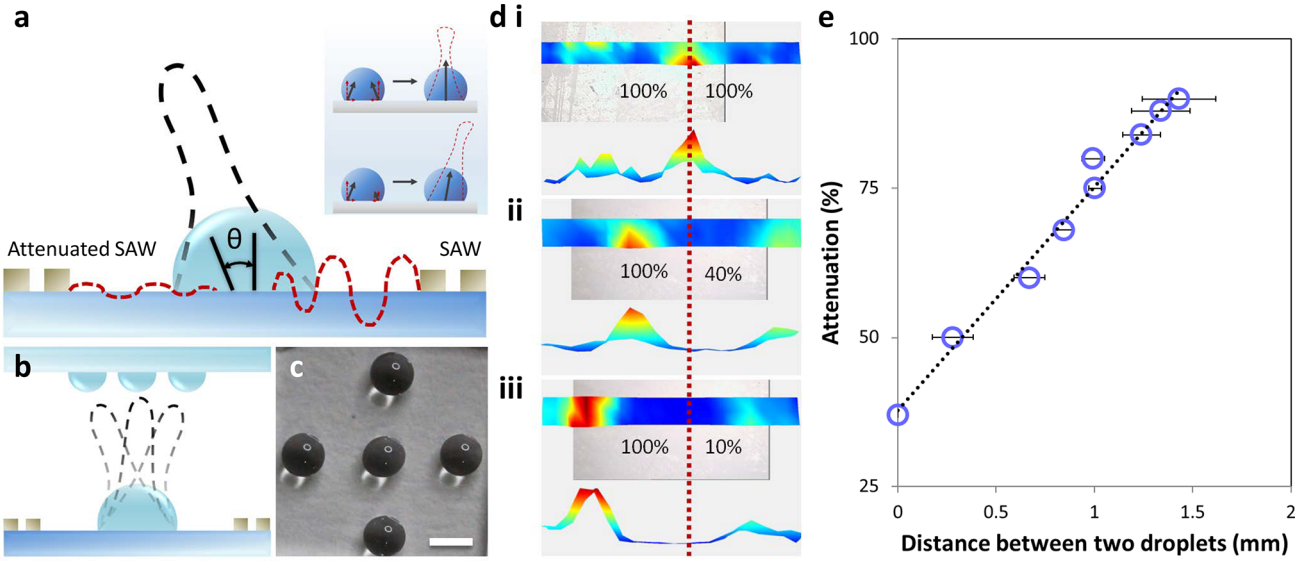

Figure 5. Schematic depiction of (a) the directional jetting scheme by applying mismatched input energies to the IDT pair, which can then be exploited to (b) print multiple droplets from the same location without necessitating repositioning either the SAW device or the target plate between each deposition event, as can be seen from part c where five droplets (one droplet in the central position directly above the parent drop on the SAW device and four neighbors) of similar volume were printed down to an interstitial spacing of approximately 1 mm. The scale bar denotes an approximate length of 1 mm. (d) Lateral root-mean-square distribution of the SAW on the substrate, as measured by the LDV. The input power to the right IDT is (i) unattenuated or attenuated by (ii) 4 and (iii) 10 dB, respectively. (e) Changing the attenuation to one IDT allows the jet angle to be altered (Table 1) which, in turn, results in a lateral shift in the print position, here represented by the edge-to-edge distance of a second droplet away from a central droplet already printed directly above the parent source drop with an unattenuated IDT pair. This obviously varies slightly depending on the height of the plate from the SAW substrate; in this case, the gap is approximately 3 mm.

Directional Printing. The dispensing time can play a critical role in the efficiency and economics of printing large-scale assays that involve massive arrays of droplets or microwells. While the speed of a single deposition step may be fast with a given technology, the total duration for printing an array may not always simply be equal to the cumulative time of these single deposition events. An example of this pertains to the ultrasonic droplet ejection technology employed by the LabCyte Echo system (LabCyte Inc., San Jose, CA) where, barring a prohibitively expensive setup that involves the use of many transducers in parallel, it is necessary to translate the transducer directly under every new target with robotic sliders and multiple positioners for every successive deposition event within the array. Even with the latest advances in robotic technology, this can still be considerably longer by at least 2 orders of magnitude of the dispensing time of a single event. While this would be true too of the current platform, albeit slightly easier and potentially faster given that the SAW chip is much smaller and lighter to mount and translate than a conventional bulk ultrasonic transducer, we turn to demonstrate the possibility of exploiting the jetting angle to carry out multiple deposition events at neighboring positions in the array from a single transducer position. In this way, the total printing time can, at least, be reduced by a factor of

$$\frac{N_A t_D + (N_A - 1)t_T}{N_A t_D + \{[N_A/(n+1)] - 1\}t_T} \approx \frac{N_A - 1}{[N_A/(n+1)] - 1} \approx n + 1 \quad (3)$$

when the requisite number of spots in the array N_A is large and the deposition time t_D is much shorter than the time it takes to mechanically or robotically translate the printhead from one position to the next t_T; n is the number of neighboring positions in the array that can be sequentially printed from a single position. It can then be seen that the total time reduction $(n + 1)t_T$ is considerable for large arrays N_A. Beyond reducing the printing time, printing multiple spots from a single printhead location also reduces translational motion which, in turn, reduces mechanical wear as well as operating and maintenance costs, especially for large industrial use where these can add up significantly.

The tuning of jetting angles has been previously reported, for example, with laser beams,[72] ultrasonic bursts,[73] and SAWs,[46,48] although these methods did not provide a means for concurrently tuning the ejected droplet dimension (or the dispensed volume) as they are generated by the jet. In addition to the ability to achieve tunability in the volume of liquid that is dispensed, as reported above, Figure 5a and Table 1 shows the possibility of tuning the jet angle θ within a range of ±22°

Table 1. Jetting Angle θ as a Function of the Attenuation of the Power to the IDTs

attenuation (dB)	jetting angle	standard error (%)
1	4.0° ± 0.4°	10.8
2	6.7° ± 0.4°	6.5
3	7.0° ± 0.1°	1.0
4	8.2° ± 0.7°	8.5
5	10.9° ± 1.1°	10.5
6	11.4° ± 0.5°	4.7
7	13.8° ± 1.1°	7.9
8	14.2° ± 0.2°	1.5
9	14.3° ± 0.3°	2.4
10	15.0° ± 1.4°	9.7

DOI: 10.1021/acs.analchem.8b05319
Anal. Chem. 2019, 91, 5621−5628

to the vertical axis with only modest errors of up to 10.8% simply by creating an asymmetric imbalance to the electrical power delivered to each of the IDTs; the variation in the error possibly arises due to slight differences in the volume and positioning of the parent drop. The underlying principle for this directional jetting can be understood more clearly from the LDV scans in Figure 5d,e which show the shift in the position of the peak SAW energy and standing waveform beneath the parent drop as the power to the opposing IDT is attenuated. The range in jetting angles is then limited by the mathematical vector summation of the angles at which the SAW leaks or diffracts from the substrate into the parent drop, the Rayleigh angle, which is given by $\sin^{-1} c_{SAW}/c_l$, wherein c_l is the speed of sound in the liquid, which for water is approximately 22 °C, from both sides.

Figure 5e then shows the position and hence distance that a second droplet can be printed away from a first central droplet directly above the parent source drop from which it is dispensed by adjusting the attenuation to a single IDT (on the opposite side to where the desired deposition position is to be located) and thus the angle of jetting θ (Table 1). Using this technique, we show in Figure 5b,c that this can be exploited to print multiple droplet neighbors; in this case, four of them, each of equal volume (±0.42 μL), although we posit that droplets of different volumes can also be deposited (simply by varying the power or pulse width as dictated above between each deposition step) from the same chip location beneath without requiring its repositioning (or the repositioning of the target plate, for that matter); for the current setup with the top plate being approximately 3 mm, we achieved consistent resolution down to 0.3 ± 0.1 mm between neighboring drops, observing that the limit of attenuation before the droplets began to overlap, for this gap size, was approximately 2 dB, equivalent to an attenuation of 37%. It should also be noted that although we have demonstrated this concept with a single IDT pair, it nevertheless is possible to increase the number of IDTs, arranged around the drop in a circular fashion, and tuning the relative power to each in order to achieve finer control in the jetting angle beyond just a single axis, in addition to the possibility of increasing either the number of neighbor droplets that can be printed or decreasing the spatial resolution between them; in such an arrangement though, the directionality of the single-crystal cut in this case has to be taken into account when calculating the relative attenuation required for each IDT.

CONCLUSION

In this work, we have developed a robust, low-cost, and user-friendly acoustomicrofluidic platform to facilitate an effective pipet-free means for rapidly, reproducibly, and precisely dispensing small volumes of liquid down to 0.22 μL with a standard error of 6.5% and CV of 11.3%. The working principle of this solid-state platform, which does not utilize mechanically moving parts commonly susceptible to failure, involves the rapid millisecond order jetting of a parent drop reservoir on the substrate of a piezoelectric chip on which a pair of SAWs are generated toward a top plate (constituting the target substrate on which the sample is to be dispensed) in order to create a liquid bridge that rapidly thins and pinches-off to leave behind a precise fraction of liquid that can be tuned primarily through the pulse width and input power to the chip.

In addition to elucidating the underlying fundamental physical mechanism that underpins this process, we also exemplify the capability of the technology through two simple experiments in the microarray-based drug discovery workflow where repetitive large-scale pipetting operations are routine, namely, serial dilution and concentration. Besides demonstrating that the sample cross-contamination is extremely low, typically below 0.3%, we also show a possible concept for considerably increasing printing speed when translating the technology for large array dispensing by utilizing a unique property of directional SAW jetting in which the jet angle can be easily tuned such that multiple drops can be sequentially dispensed without requiring repositioning of the chip. While reducing the need to robotically translate the chip by a factor of 4 (in this case) is negligible in terms of time for a few dispensing operations, this could however add up to be significant in cost for massively large parallel microarray operations, not just in terms of speed but also maintenance costs by minimizing the number of mechanical translation events. Moreover, the SAW device, given its size, can easily be incorporated into a printhead on a translation stage for automated control and/or integrated for parallel operation for massively parallel, individually addressable, sequential, or simultaneous operation on-demand through an integrated array-based platform we have recently developed.[54]

AUTHOR INFORMATION

Corresponding Author

*E-mail: leslie.yeo@rmit.edu.au Phone: + 61 3 9925 2596.

ORCID

Leslie Y. Yeo: 0000-0002-5949-9729

Notes

The authors declare no competing financial interest.

ACKNOWLEDGMENTS

A.R.R. is grateful for an RMIT University Vice-Chancellor's Postdoctoral Fellowship. L.Y.Y. acknowledges funding from the Australian Research Council (ARC) through Discovery Project (Grant DP170101061).

REFERENCES

(1) Janasek, D.; Franzke, J.; Manz, A. *Nature* **2006**, *442*, 374−380.
(2) Yeo, L.; Chang, H.; Chan, P.; Friend, J. *Small* **2011**, *7*, 12−48.
(3) Sackmann, E. K.; Fulton, A. L.; Beebe, D. J. *Nature* **2014**, *507*, 181−189.
(4) Stone, H.; Stroock, A.; Ajdari, A. *Annu. Rev. Fluid Mech.* **2004**, *36*, 381−411.
(5) Friend, J.; Yeo, L. *Rev. Mod. Phys.* **2011**, *83*, 647−704.
(6) Ding, X.; Li, P.; Lin, S.-C. S.; Stratton, Z. S.; Nama, N.; Guo, F.; Slotcavage, D.; Mao, X.; Shi, J.; Costanzo, F.; Huang, T. J. *Lab Chip* **2013**, *13*, 3626−3649.
(7) Yeo, L. Y.; Friend, J. R. *Annu. Rev. Fluid Mech.* **2014**, *46*, 379−406.
(8) Destgeer, G.; Sung, H. J. *Lab Chip* **2015**, *15*, 2722−2738.
(9) Go, D. B.; Atashbar, M. Z.; Ramshani, Z.; Chang, H.-C. *Anal. Methods* **2017**, *9*, 4112−4134.
(10) Destgeer, G.; Lee, K. H.; Jung, J. H.; Alazzam, A.; Sung, H. J. *Lab Chip* **2013**, *13*, 4210−4216.
(11) Franke, T.; Braunmüller, S.; Schmid, L.; Wixforth, A.; Weitz, D. A. *Lab Chip* **2010**, *10*, 789−794.
(12) Lin, S.-C. S.; Mao, X.; Huang, T. J. *Lab Chip* **2012**, *12*, 2766−2770.
(13) Behrens, J.; Langelier, S.; Rezk, A.; Lindner, G.; Yeo, L.; Friend, J. *Lab Chip* **2015**, *15*, 43−46.

DOI: 10.1021/acs.analchem.8b05319
Anal. Chem. 2019, 91, 5621−5628

(14) Ren, L.; Chen, Y.; Li, P.; Mao, Z.; Huang, P.-H.; Rufo, J.; Guo, F.; Wang, L.; McCoy, J. P.; Levine, S. J.; Huang, T. J. *Lab Chip* **2015**, *15*, 3870−3879.
(15) Destgeer, G.; Ha, B. H.; Park, J.; Jung, J. H.; Alazzam, A.; Sung, H. J. *Anal. Chem.* **2015**, *87*, 4627−4632.
(16) Ma, Z.; Zhou, Y.; Collins, D. J.; Ai, Y. *Lab Chip* **2017**, *17*, 3176−3185.
(17) Ung, W. L.; Mutafopulos, K.; Spink, P.; Rambach, R. W.; Franke, T.; Weitz, D. A. *Lab Chip* **2017**, *17*, 4059−4069.
(18) Collins, D. J.; Devendran, C.; Ma, Z.; Ng, J. W.; Neild, A.; Ai, Y. *Sci. Adv.* **2016**, *2*, E1600089.
(19) Wu, M.; Mao, Z.; Chen, K.; Bachman, H.; Chen, Y.; Rufo, J.; Ren, L.; Li, P.; Wang, L.; Huang, T. J. *Adv. Funct. Mater.* **2017**, *27*, 1606039.
(20) Wixforth, A.; Strobl, C.; Gauer, C.; Toegl, A.; Scriba, J.; v. Guttenberg, Z. *Anal. Bioanal. Chem.* **2004**, *379*, 982−991.
(21) Tan, M. K.; Friend, J. R.; Yeo, L. Y. *Lab Chip* **2007**, *7*, 618−625.
(22) Renaudin, A.; Galopin, E.; Thomy, V.; Druon, C.; Zoueshtiagh, F. *Phys. Fluids* **2007**, *19*, 091111.
(23) Brunet, P.; Baudoin, M.; Matar, O. B.; Zoueshtiagh, F. *Phys. Rev. E* **2010**, *81*, 036315.
(24) Baudoin, M.; Brunet, P.; Matar, O. B.; Herth, E. *Appl. Phys. Lett.* **2012**, *100*, 154102.
(25) Bussonnière, A.; Baudoin, M.; Brunet, P.; Matar, O. B. *Phys. Rev. E: Stat. Phys., Plasmas, Fluids, Relat. Interdiscip. Top.* **2016**, *93*, 053106.
(26) Guttenberg, Z.; Rathgeber, A.; Keller, S.; Rädler, J. O.; Wixforth, A.; Kostur, M.; Schindler, M.; Talkner, P. *Phys. Rev. E* **2004**, *70*, 056311.
(27) Girardo, S.; Cecchini, M.; Beltram, F.; Cingolani, R.; Pisignano, D. *Lab Chip* **2008**, *8*, 1557−1563.
(28) Schneider, M. F.; Guttenberg, Z.; Schneider, S. W.; Sritharan, K.; Myles, V. M.; Pamukci, U.; Wixforth, A. *ChemPhysChem* **2008**, *9*, 641−645.
(29) Tan, M. K.; Yeo, L. Y.; Friend, J. R. *EPL* **2009**, *87*, 47003.
(30) Masini, L.; Cecchini, M.; Girardo, S.; Cingolani, R.; Pisignano, D.; Beltram, F. *Lab Chip* **2010**, *10*, 1997−2000.
(31) Schmid, L.; Wixforth, A.; Weitz, D. A. *Microfluid. Nanofluid.* **2012**, *12*, 229−235.
(32) Langelier, S. M.; Yeo, L. Y.; Friend, J. *Lab Chip* **2012**, *12*, 2970−2976.
(33) Johansson, L.; Enlund, J.; Johansson, S.; Katardjiev, I.; Yantchev, V. *Biomed. Microdevices* **2012**, *14*, 279−289.
(34) Miansari, M.; Friend, J. R. *Adv. Funct. Mater.* **2016**, *26*, 7861−7872.
(35) Li, H.; Friend, J. R.; Yeo, L. Y. *Biomed. Microdevices* **2007**, *9*, 647−656.
(36) Shilton, R.; Tan, M. K.; Yeo, L. Y.; Friend, J. R. *J. Appl. Phys.* **2008**, *104*, 014910.
(37) Shilton, R. J.; Travagliati, M.; Beltram, F.; Cecchini, M. *Adv. Mater.* **2014**, *26*, 4941−4946.
(38) Destgeer, G.; Jung, J. H.; Park, J.; Ahmed, H.; Sung, H. J. *Anal. Chem.* **2017**, *89*, 736−744.
(39) Tan, M.; Friend, J.; Yeo, L. *Phys. Rev. Lett.* **2009**, *103*, 024501.
(40) Qi, A.; Yeo, L. Y.; Friend, J. R. *Phys. Fluids* **2008**, *20*, 074103.
(41) Ho, J.; Tan, M. K.; Go, D. B.; Yeo, L. Y.; Friend, J. R.; Chang, H.-C. *Anal. Chem.* **2011**, *83*, 3260−3266.
(42) Heron, S. R.; Wilson, R.; Shaffer, S. A.; Goodlett, D. R.; Cooper, J. M. *Anal. Chem.* **2010**, *82*, 3985−3989.
(43) Winkler, A.; Harazim, S. M.; Menzel, S. B.; Schmidt, H. *Lab Chip* **2015**, *15*, 3793−3799.
(44) Winkler, A.; Harazim, S.; Collins, D. J.; Brünig, R.; Schmidt, H.; Menzel, S. B. *Biomed. Microdevices* **2017**, *19*, 9.
(45) Vuong, T.; Qi, A.; Muradoglu, M.; Cheong, B. H.-P.; Liew, O. W.; Ang, C. X.; Fu, J.; Yeo, L.; Friend, J.; Ng, T. W. *Soft Matter* **2013**, *9*, 3631−3639.
(46) Bourquin, Y.; Wilson, R.; Zhang, Y.; Reboud, J.; Cooper, J. *Adv. Mater.* **2011**, *23*, 1458−1462.
(47) Fu, C.; Quan, A.; Luo, J.; Pang, H.; Guo, Y.; Wu, Q.; Ng, W.; Zu, X.; Fu, Y. *Appl. Phys. Lett.* **2017**, *110*, 173501.
(48) Fu, Y.; Luo, J.; Nguyen, N.; Walton, A.; Flewitt, A.; Zu, X.; Li, Y.; McHale, G.; Matthews, A.; Iborra, E.; Du, H.; Milne, W. *Prog. Mater. Sci.* **2017**, *89*, 31−91.
(49) Castro, J.; Ramesan, S.; Rezk, A.; Yeo, L. *Soft Matter* **2018**, *14*, 5721−5727.
(50) Demirci, U.; Montesano, G. *Lab Chip* **2007**, *7*, 1139−1145.
(51) Bhattacharjee, P.; McDonnell, A.; Prabhakar, R.; Yeo, L.; Friend, J. *New J. Phys.* **2011**, *13*, 023005.
(52) McDonnell, A. G.; Jason, N. N.; Yeo, L. Y.; Friend, J. R.; Cheng, W.; Prabhakar, R. *Soft Matter* **2015**, *11*, 8076−8082.
(53) McDonnell, A. G.; Gopesh, T. C.; Lo, J.; O'Bryan, M.; Yeo, L. Y.; Friend, J. R.; Prabhakar, R. *Soft Matter* **2015**, *11*, 4658−4668.
(54) Rezk, A.; Ramesan, S.; Yeo, L. *Lab Chip* **2018**, *18*, 406−411.
(55) Glass, N.; Tjeung, R.; Chan, P.; Yeo, L.; Friend, J. *Biomicrofluidics* **2011**, *5*, 036501.
(56) Cheng, N.-S. *Ind. Eng. Chem. Res.* **2008**, *47*, 3285−3288.
(57) Volk, A.; Kähler, C. J. *Exp. Fluids* **2018**, *59*, 1432−1114.
(58) Mosmann, T. *J. Immunol. Methods* **1983**, *65*, 55−63.
(59) Josserand, C.; Thoroddsen, S. *Annu. Rev. Fluid Mech.* **2016**, *48*, 365−391.
(60) Craster, R. V.; Matar, O. K. *Rev. Mod. Phys.* **2009**, *81*, 1131−1198.
(61) Kalliadasis, S.; Chang, H.-C. *Phys. Fluids* **1994**, *6*, 12−23.
(62) Kalliadasis, S.; Chang, H.-C. *Ind. Eng. Chem. Res.* **1996**, *35*, 2860−2874.
(63) Yeo, L. Y.; Chang, H.-C. *Phys. Rev. E* **2006**, *73*, 011605.
(64) Clanet, C.; Béguin, C.; Richard, D.; Quéré, D. *J. Fluid Mech.* **1999**, *517*, 199−208.
(65) Fedorchenko, A. I.; Wang, A.-B.; Wang, Y.-H. *Phys. Fluids* **2005**, *17*, 093104.
(66) Eggers, J.; Fontelos, M. A.; Josserand, C.; Zaleski, S. *Phys. Fluids* **2010**, *22*, 062101.
(67) Choi, D.; Lee, H.; Im, D.; Kang, I.; Lim, G.; Kim, D.; Kang, K. *Sci. Rep.* **2013**, *3*, 2037.
(68) Fan, J.; Men, Y.; Hao Tseng, K.; Ding, Y.; Ding, Y.; Villarreal, F.; Tan, C.; Li, B.; Pan, T. *Biomicrofluidics* **2018**, *12*, 034107.
(69) Walker, G. M.; Monteiro-Riviere, N.; Rouse, J.; O'Neill, A. T. *Lab Chip* **2007**, *7*, 226−232.
(70) Mao, Y.; Pan, Y.; Li, X.; Li, B.; Chu, J.; Pan, T. *Lab Chip* **2018**, *18*, 2720−2729.
(71) Alhasan, L.; Qi, A.; Rezk, A. R.; Yeo, L. Y.; Chan, P. P. *Integr. Biol.* **2016**, *8*, 12−20.
(72) Padilla-Martinez, J.; Ramirez-San-Juan, J.; Berrospe-Rodriguez, C.; Korneev, N.; Aguilar, G.; Zaca-Moran, P.; Ramos-Garcia, R. *Appl. Opt.* **2017**, *56*, 7167−7173.
(73) Gerold, B.; Glynne-Jones, P.; McDougall, C.; McGloin, D.; Cochran, S.; Melzer, A.; Prentice, P. *Appl. Phys. Lett.* **2012**, *100*, 024104.

DOI: 10.1021/acs.analchem.8b05319
Anal. Chem. 2019, 91, 5621−5628